Soft Matter

RSC Publishing

PAPER

View Article Online
View Journal | View Issue

# Rolling particle lithography by soft polymer microparticles†

Cite this: *Soft Matter*, 2013, **9**, 2206

Francesca Di Benedetto,‡[a] Vito Fasano,[bc] Luana Persano,[ab] Claudio Maruccio,[e] Elisa Mele,§[b] Giovanni Potente,[a] David A. Weitz,[d] Laura De Lorenzis[e] and Dario Pisignano*[abc]

Received 9th October 2012
Accepted 10th December 2012

DOI: 10.1039/c2sm27327f

**www.rsc.org/softmatter**

Elastomeric polymeric microspheres are employed as a direct-writing tool for the continuous delivery of molecular materials. The mechanical properties enabling patterning are investigated and modelled. The proposed approach provides a low cost and versatile lithographic method for transferring features with real-time dynamic control.



## Introduction

Patterning functional materials is of paramount importance for many fields of science and technology, being the crucial step in the fabrication of integrated circuits, miniaturized sensors, biodiagnostic devices, and micro-optical components. Among the most appealing methods developed to create patterns,[1] printing approaches such as microcontact printing (μCP)[2–4] and edge transfer lithography[5] are based on a template (stamp) with a prearranged design that is duplicated while contacting a substrate. These methods have strong potential for a widespread use, since they are compatible with a wide variety of target systems (molecules, proteins, colloids, polymers, cells, *etc.*) and substrates (rigid and flexible). The evolution of these approaches has led to the development of dynamic, continuous printing strategies for achieving high velocity and large area pattern formation. Whitesides and co-workers replaced flat poly(dimethylsiloxane) (PDMS) stamps with a cylinder rolling over the substrate for generating sub-μm features of self assembled monolayers.[6] Another dynamic μCP method using conventional stamps moving or jumping during the lithographic process for fabricating polymer-brush microstructures has been recently proposed.[7]

Unfortunately, the design flexibility and performance of contact printing techniques are strongly affected by the characteristics of the stamp that binds the geometry, the resolution and the spatial extension of the final pattern.[8] The availability of templates often remains a bottleneck for developing next-generation, flexible lithographic processes, since their fabrication generally requires moderately advanced micro-nanofabrication techniques and not always accessible clean-room facilities. More importantly, most of the printing processes follow the "one template-one pattern" paradigm, even minor changes in the pattern design necessarily leading to the fabrication of a dedicated template. For these reasons the development of alternative printing strategies is desirable, having significant impact on the operating time, production costs, and pattern flexibility. For instance, PDMS-coated dip pen nanolithography (DPN)[9] stamp tips have been developed, allowing to deliver molecular inks on surfaces with very high resolution (sub-100 nm) and typical writing speed below or of the order of 1 μm $s^{-1}$.[10]

Here, we present a complementary, innovative printing method, the rolling particle soft lithography (RPL), that overcomes the need for specific templates using elastomeric microparticles rolling on surfaces to produce features over large areas (few $cm^2$), with high pattern design flexibility, and using simple fabrication equipment. This approach takes advantage of the inherently favorable elastic nature of polymeric microparticles as a direct-writing tool for the continuous delivery of molecular materials, with real-time dynamic control over the size and complexity of the transferred features. We demonstrate the application of RPL for realizing interconnected or multiple-chemistry patterns by exploiting the volume of the microparticle as inkwells containing different molecules.

[a]*National Nanotechnology Laboratory of Istituto Nanoscienze-CNR, Università del Salento, via Arnesano, I-73100 Lecce, Italy. E-mail: dario.pisignano@unisalento.it; Fax: +39 0832 298146; Tel: +39 0832 298104*

[b]*Center for Biomolecular Nanotechnologies, Istituto Italiano di Tecnologia (I.I.T.), via Barsanti 1, I-73010 Arnesano-LE, Italy*

[c]*Dipartimento di Matematica e Fisica "Ennio De Giorgi", Università del Salento, via Arnesano, I-73100 Lecce, Italy*

[d]*Department of Physics & School of Engineering and Applied Sciences, Harvard University, Cambridge, Massachusetts 02138, USA*

[e]*Dipartimento di Ingegneria dell'Innovazione, Università del Salento, via Arnesano, I-73100 Lecce, Italy*

† Electronic supplementary information (ESI) available. See DOI: 10.1039/c2sm27327f

‡ Present address: ENEA, Technical Unit of Material Technologies Brindisi, Strada Statale 7 Appia km. 706, 72100 Brindisi, Italy.

§ Present address: Nanophysics, Istituto Italiano di Tecnologia (I.I.T.), via Morego 30, 16163 Genova, Italy.

## Results and discussion

The key features of RPL are an inked, elastomeric microsphere and an external setup able to impart a controlled rotational movement to such a particle. We easily generate elastomeric microspheres with desired diameters in the range of 50–220 μm by calibrating the operation flows of PDMS microfluidic devices[11–13] (see ESI for details†) (Fig. 1). In this study, we use two different classes of microfluidic chips (A and B) with width of the central inlet channel of 30 and 100 μm, respectively. Under appropriate flow rate conditions, a jet is formed at the junction between the dispersed and the continuous-phase flow (Fig. 1a–c). The higher affinity of the continuous phase to the sidewall of the plasma-oxidized channel and the strong contraction coupled with the highly accelerating continuous phase allow the stream of PDMS to be completely surrounded by the aqueous phase and elongated until breakup occurs.[14] Afterwards, the PDMS droplets in the aqueous phase are collected into a vial and heated at 65 °C for 12 hours, producing isolated spherical solid microparticles (Fig. 1d–f). The formation of the hexagonal close-packed structure, which self-assembles after the evaporation of the continuous aqueous phase, is evidence of the good uniformity of the size of the resultant microparticles. In some cases, the shape of the particles is not perfectly spherical (Fig. 1e), due to formation of pores and slight deformations during solidification and drying. In fact, the relatively high viscosity of PDMS can induce entrapment of air microbubbles within the polymer matrix, thus generating empty volumes that can collapse during solvent evaporation. Overall, the particle size is easily tailored since it decreases monotonically upon increasing the flow-rate ($Q_c$) of the continuous phase (Fig. 1g). Particles with diameters well-above 220 μm can also be obtained by chip B, under conditions of very low flow rates ($Q_c \leq 5$ μL min$^{-1}$ and dispersed phase flow rate $Q_d = 0.5$ μL min$^{-1}$), determining low capillary numbers and complete absence of Rayleigh–Plateau instabilities.

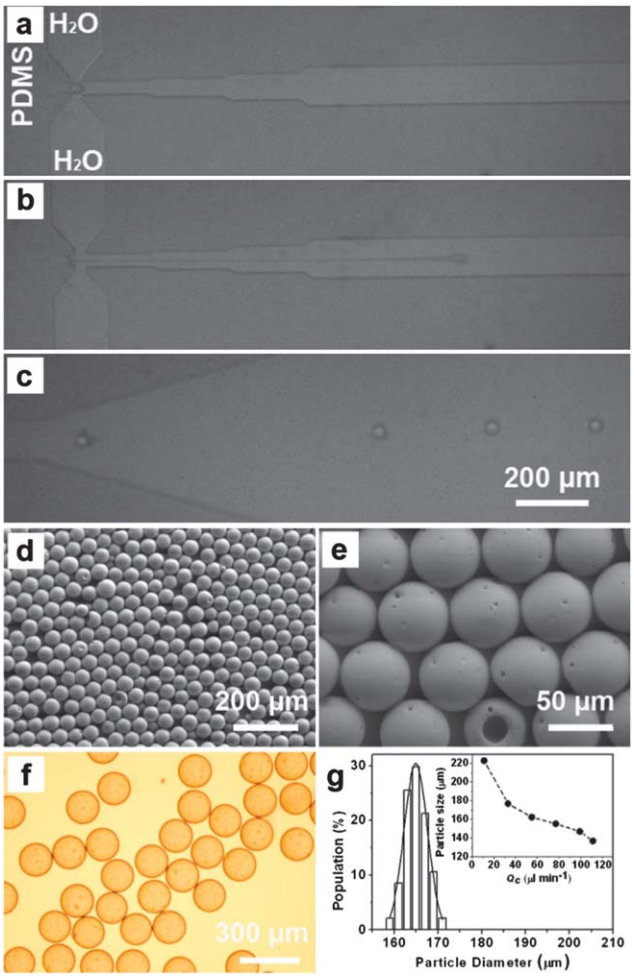


**Fig. 1** (a–c) High-speed micrographs (250 fps) at the same magnification, showing the production of PDMS droplets in water, generated in a dripping regime by using a flow-focusing device, with a production rate of about 1 s$^{-1}$. The dispersed phase (flow rate, $Q_d = 1$ μL min$^{-1}$) is squeezed by two streaming counter aqueous flows of the continuous phase (flow rate, $Q_c = 3$ μL min$^{-1}$), forcing drops to detach. (c) Collection chamber. PDMS microparticles obtained by a flow-focusing (d and e) and by an intersecting-microchannel device (f and g). (d and e) SEM micrographs at different magnifications of the particles after thermal polymerization. (f) Optical micrograph of PDMS microdroplets in water, generated by flow rates of $Q_d = 1$ μL min$^{-1}$ and $Q_c = 55$ μL min$^{-1}$. (g) Typical size distribution of PDMS particles. The size distribution is well fitted by a Gaussian curve with a full width at half maximum of about 6 μm. Inset: average particle diameter *vs.* rate of the continuous phase. $Q_d = 1$ μL min$^{-1}$.

The elastomeric microspheres are then directly used for RPL. In a typical experiment, the particles are firstly immersed in an ink solution, and then dried by a $N_2$ stream and rolled on the target surface to be patterned. To impart the rolling motion, single particles are carefully placed between the substrate and an upper glass plate, which is moved by a micrometer stage controllable along three orthogonal directions (Fig. 2a). A calibrated pressure is applied to the particle through the movement of the upper plate along the $z$ direction. The conformal contact between glass and PDMS enables the $x$–$y$ translational motion of the plate, which can be manual or motorized, to be easily transmitted to the rolling microparticle (Fig. 2b–d, extracted from Movie S1 available as ESI†), which locally delivers the ink, thus producing patterns with microscale resolution. Several factors are involved in the RPL pattern formation. As for other contact printing approaches, the mechanism responsible for ink transfer from the elastomeric element to the underlying substrate may depend on the specifically used molecules, on the substrate-ink and elastomer–ink interactions, and on the environmental conditions.[15,16] Local liquid delivery and spreading, vapor and mass transport are possible pathways that determine pattern formation during printing, and the ink vapor pressure affects the interaction with the substrate mediating surface coverage.[15] In particular, the presence of water on the surface, as an effect of the relative ambient humidity (RH), can be detrimental to the final pattern quality, reducing the ink–substrate interaction and inducing a lateral spreading of the ink molecules along the water meniscus formed at the interface between PDMS and the substrate.[16] For the sake of comparison, we recall that the role of humidity is also recognized to limit the resolution achievable in DPN.[17] Here RH is kept below 30% at room temperature as the best ambient condition to carry out RPL processes.

Importantly, the elastomeric character of the particle allows features of different resolutions to be delivered by means of a

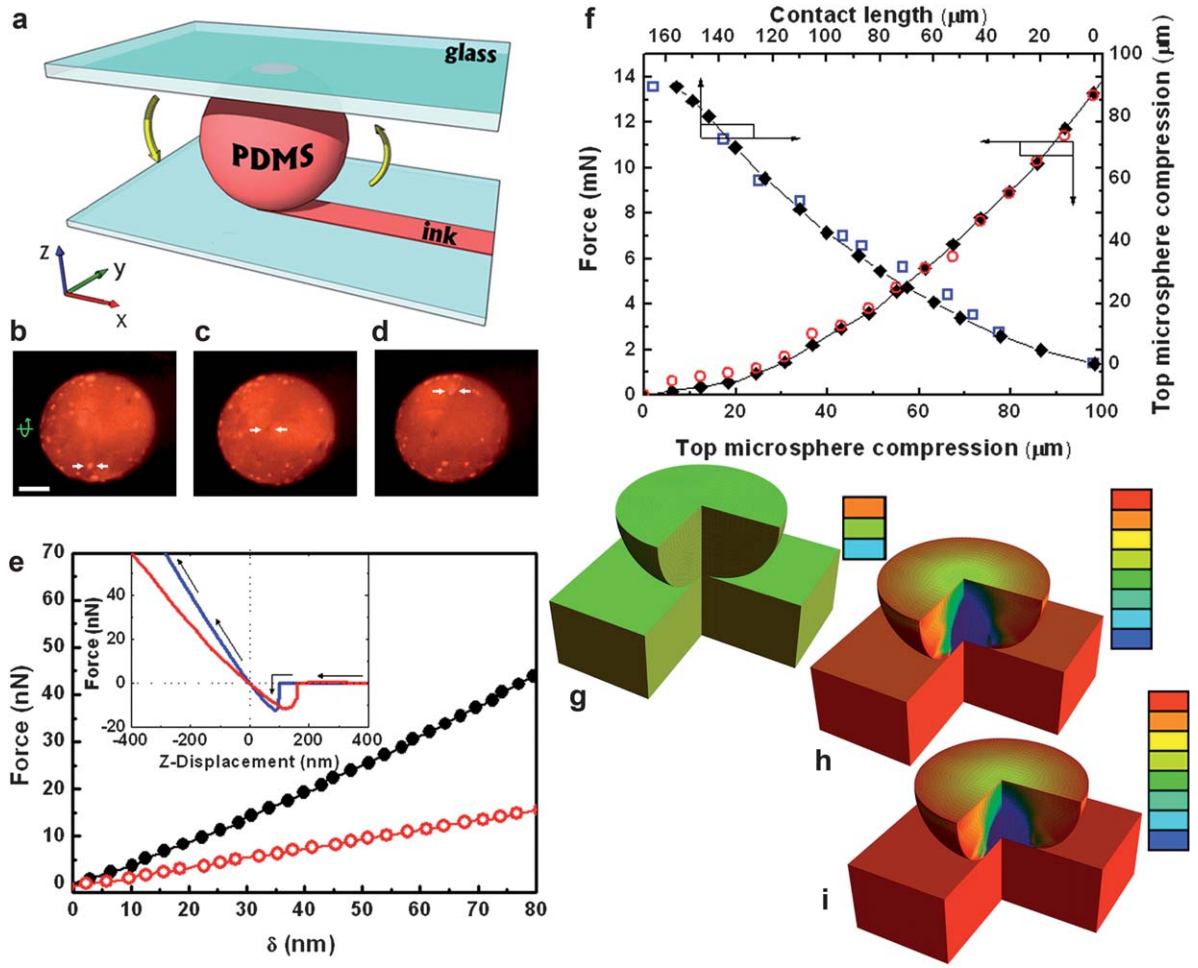


**Fig. 2** (a) Schematic view of the printing process by RPL. (b–d) Fluorescent micrographs of a rolling particle at various time instants. The arrows indicate a fluorescent feature on the sphere surface, allowing easy visualization of the rotation. Scale bar = 40 μm. (e) Force–nanoindentation plots for individual PDMS microspheres (empty dots) and films (full dots). Inset: force *vs.* piezo-displacement curve for individual PDMS microspheres (red line) and films (blue line). The arrows indicate the tip-approaching direction. (f) Applied compression force *vs.* top displacement of an elastomeric particle (open circles, left-bottom axes, sphere diameter = 600 μm), and width of the patterned features *vs.* particle top displacement (open squares, right-top axes, sphere diameter = 165 μm). The width of patterned features reported here provides the information on the resulting patterns that can be modulated with the deformation. Superimposed diamond-line curves are numerical results obtained by an elastic modulus of 0.8 MPa. (g–i) Calculated Cauchy stress in the vertical direction, $\sigma_{zz}$, plotted on the deformed mesh of a half elastomeric sphere, upon no vertical deformation (g), and under a top displacement of 50 μm (h) and 100 μm (i), respectively. Minimum and maximum compressive stress corresponding to the vertical color scales are $2.2 \times 10^4$ to $1.3 \times 10^5$ N m$^{-2}$ (g), $2.7 \times 10^3$ to $7.5 \times 10^4$ N m$^{-2}$ (h), and $1.1 \times 10^4$ to $1.6 \times 10^5$ N m$^{-2}$ (i), respectively.

single writing tool, controlling the PDMS deformation through the application of calibrated pressures. This approach permits to tailor the resulting contact area with the underlying surface, because particles can be compressed and then rolled while being deformed. The particle elastic character is initially quantified at very small deformations (particle top displacement, $\delta$), by force–displacement curves using a scanning probe tip (Fig. 2e). Fitting the linear part of the load-displacement curves in the region of small indentation ($\delta \leq 10$ nm), according to Hertz's model, the relationship between the normal load, $F$, applied to the elastic sphere, and the resulting deformation is given by $F = (4/3)R^{*1/2}E^{*}\delta^{3/2}$. Here, $R^{*}$ and $E^{*}$ are the relative radius of curvature and the combined strain modulus of the tip (1) and of the sample (2), respectively, namely ${R^{*}}^{-1} = {R_1}^{-1} + {R_2}^{-1}$ and ${E^{*}}^{-1} = (1 - {\nu_1}^2){E_1}^{-1} + (1 - {\nu_2}^2){E_2}^{-1}$. For our RPL spheres, we find a compressive modulus of about 4 MPa upon nanoindentation, in agreement with the values reported for similar polymeric systems[18,19] and quite lower than reference PDMS films[20] for which we measure a modulus of 11 MPa.

In order to investigate the μm-scale deformation regimes needed for RPL, we carry out compression experiments applying calibrated weights onto the elastomeric microspheres, and analyze the resulting particle behaviour. We use spheres with initial diameters ($d$) of 165 and 600 μm, undergoing relative deformations [$\Delta_R \sim (d - \delta)/d \times 100$] up to about 50%, as determined by optical microscopy (Fig. 2f). Relative deformations of the order of 10% correspond to applied loads in the mN range. The size of the resulting printed features monotonically increases upon increasing the PDMS deformation, varying from 35 μm (minimum value corresponding to the almost undeformed particle) to 164 μm, with an almost 5-fold overall resolution change, for a particle with $d$ = 165 μm (Fig. 2f). To

 

determine the material properties, the system is modelled numerically with the finite element method, thus exploiting an inverse analysis of the observed mechanical response. In the model, the PDMS particle is considered as an elastic solid with a hyperelastic neo-Hooke constitutive behavior,[21] while the loading and support platens are assumed rigid. We find that the experimental deformation of the overall particle at the microscale is well-described by an elastic modulus of 0.8 MPa (diamond-line curves in Fig. 2f). Fig. 2g–i also show the contours of the Cauchy stress in the vertical ($z$) direction, $\sigma_{zz}$, plotted on the deformed mesh of a half sphere (with a cut to illustrate the internal stress distribution) for different values of the displacement factor, $\delta/\delta_{MAX}$, where $\delta_{MAX}$ is the maximum displacement. The sphere is seen to undergo a quite large deformation regime, which clearly invalidates the use of linear analytical theories such as that by Hertz to predict the full range of response.

Therefore, RPL is a rapid prototyping process allowing the pattern resolution to be amply varied at the microscale in a single patterning run, without fabricating different templates. Due to the well-established pattern transfer capability of μCP methods,[22] it is likely that the ultimate feature dimension transferrable, by high molar mass inks avoiding diffusion, will be below 1 μm, related to the Young's modulus and to the ultimate size of elastomeric particles reliably produced by microfluidic devices.[23]

Furthermore, the writing process is fast, a particle linear speed of 60 μm $s^{-1}$ allows a layer of molecules to be locally delivered, as determined by temporal sequences of collected micrographs. The writing rate could be further increased, up to a limit contact duration in the millisecond regime,[24] also affecting the final resolution of the transferred patterns. Higher rates would demand an appropriate tuning of the ink properties (such as diffusion and solution viscosity), in order to assure uniform delivery of organic molecules.[3] An improvement of RPL with respect to mold-assisted μCP is in producing patterns of considerable complexity. By controlling the particle motion, the generated patterns can be aligned on pre-defined geometries, metal electrodes (Fig. 3a–f and ESI†), *etc.*, with a registration accuracy of a few μm (due to the possible distortions of PDMS particles).[25] Various greek patterns realized by solutions of different fluorescent dyes as inks are shown in Fig. 3g–j. Patterns in Fig. 3g–i are obtained by using a single rolling sphere on glass, without any surface treatments to promote the ink transfer. The transfer of fluorescent dyes is highly localized at the sites of contact between the compressed RPL particle and the target substrate, highlighting good mechanical stability of the sphere and absence of appreciable surface diffusion of the adsorbed molecules. A large number of patterns (over an area of about 1 $cm^2$) can be realized by a single inking process without any measurable reduction of the writing quality. This suggests that inking by immersion causes the dye molecules to diffuse inside the PDMS particles,[10,26] which then serve as a continuously feeding inkwell during pattern transfer. This mechanism allows the generation of large area patterns without the realignment steps needed for ink replenishment on printing elements. With our experimental setup, during the process the ink is also delivered to the upper glass slide. This, together with a non-uniform imbibition of the dyes into the particle body, can lead to a higher consumption rate of the ink and locally dishomogeneous patterned features. Approaches to provide a continuous ink flow to the particle can be useful in this respect, such as in fountain-pen methods.[27] These can be implemented by the integration of a microfluidic system in the upper glass slide, able to connect the rolling particle to a large ink reservoir.

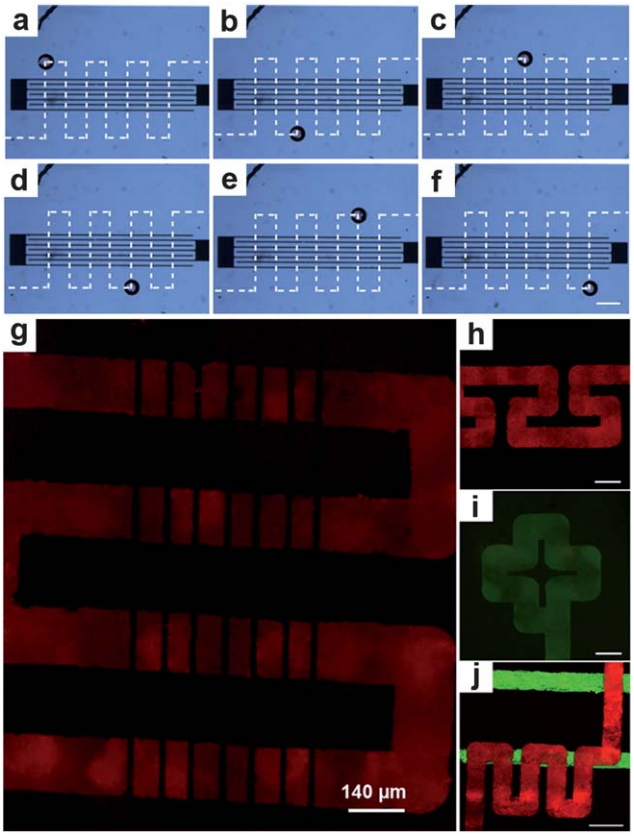


**Fig. 3** (a–f) Optical micrographs of a particle at various time instants, rolling on pre-defined interdigitated metal electrodes. Marker = 280 μm. From (a) to (f), time = 75 s, 150 s, 212.5 s, 275 s, 337.5 s, and 400 s. The average velocity of the microsphere is 20 μm $s^{-1}$. (g) Corresponding rhodamine pattern fluorescence. (h and i) Fluorescence micrographs of dye molecules patterned on glass using a single rolling particle inked by rhodamine (h) and coumarin (i). Scale bar: 100 μm. (j) Confocal micrograph of a pattern with two different dyes subsequently delivered onto the same substrate. Scale bar: 160 μm.

Multicomponent arbitrary patterns of different molecules are also realized (Fig. 3j). Both sequential and parallel approaches may be used for printing different ink species onto the same surface by RPL. In the former procedure, different particles are exploited for transferring various inks to a single substrate by successive rolling steps. We do not find significant loss of contrast or resolution, indicating unidirectional delivery of molecules as in sequential μCP.[4] In the second case, multicomponent patterns can be obtained by running many microspheres (with various inks) in parallel, using suitable microstructured pressing slides to drive the particles, which would speed up the process, especially for large area applications. Moreover, arbitrary, complex paths are easily produced by moving the inked particles in a highly controlled way, using a

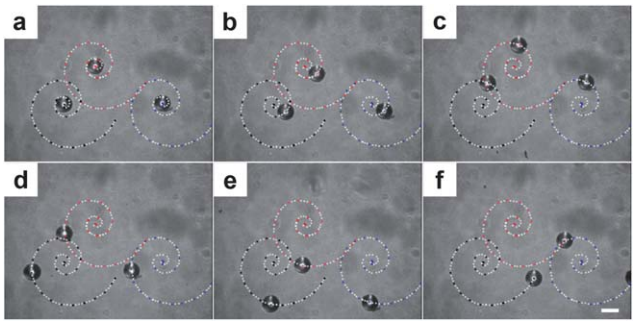


**Fig. 4** Micrographs of multiple particles at various time instants, while being controlled along a spiral pattern. Each spiral pattern is defined by $x = ae^{bt}$ cos $t$ and $y = ae^{bt}$ sin $t$, where $x$ and $y$ indicate the two Cartesian, planar coordinates whose origin is in the spiral center, $t$ is time, $a = 0.5$ μm and $b = 0.7$ s$^{-1}$. From (a) to (f), time = 0 s, 35 s, 50 s, 75 s, 95 s, and 120 s. Microsphere average velocity ≅ 10 μm s$^{-1}$. Marker = 60 μm.

piezo-controlled automated stage, and multiple particles can be moved simultaneously (Fig. 4, details in the ESI†). More in general, while RPL is suitable to print long lines and complex but continuous features, patterning dots or short segments can be more difficult. To this aim, one would need a non-continuous contact between the ink-delivering rolling particles and the target substrate, which can be obtained by microstructured elastomeric elements as in other μCP methods with rolling stamps.[6] Importantly, RPL can be applied to a wide variety of small molecules able to diffuse inside the PDMS matrix[10,26] and to be transferred onto a substrate. Such molecules can then be used as binding agents for achieving spatially controlled covalent or electrostatic immobilization of functionalized biomolecules or other organic compounds including polymers.

## Conclusions

In conclusion, RPL using elastomeric microparticles is a printing technique which is remarkable for its simplicity, versatility, and low cost. The resolution of printed patterns is not strictly limited by the native size of polymer microspheres, but can instead be tailored by the controllable deformation of the elastomeric particles, increasing the lithography flexibility and opening new perspectives for overcoming the "one template-one pattern" paradigm. The realization of complex patterns by multicomponent RPL has potential applications in different fields, such as patterns of biomolecules and light-emitting organics for biotechnology and optoelectronics.

## Experimental section

### Materials

All materials are obtained commercially and used as received. The Zonyl® fluorosurfactant [$(C_2H_4O)_x(CF_2)_yC_2H_5FO$], rhodamine (red-fluorescent dye) and coumarin (green-fluorescent dye) are purchased from Sigma Aldrich. Dye solutions are prepared using water and absolute ethanol. Microparticles are formed by PDMS (Sylgard 184, Dow Corning).

### Realization of microparticles

Two master structures (A and B) are fabricated starting from a photoresist pattern generated by optical lithography. The first master (for device A, flow-focusing), used for producing particles with a diameter of 50 μm, has three flow-focusing channels with widths of 30 μm (central inlet) and 150 μm (side channels) and a height of 37 μm, connected to a straight channel with a rectangular cross-section 45 μm × 37 μm which gradually increases up to 150 μm in order to slow down the flow rate. The second master (for device B, with inlet microchannels intersecting at about 45°), used for the realization of particles with a diameter above 100 μm, has three flow-focusing channels with a width of 100 μm and height of 80 μm, connected to a straight channel with a rectangular cross-section 350 μm × 80 μm and length of about 2 cm. The masters are replicated using the Sylgard 184 base and curing agent in a ratio of 9 : 1 in weight. The resulting PDMS replicas and glass substrates are oxidized *via* oxygen plasma discharge with a plasma reactor (Tucano, Gambetti Kenologia), and bonded irreversibly by using a power of 50 Watt over 15 s. To prevent the organic phase from coming in contact with the plasma-oxidized PDMS walls of the device, the channels are filled with water immediately after device sealing[28] until the introduction of the dispersed phase. The microfluidic devices are used to generate elastomeric particles for at least 8 hours of continuous operation. During the experiments we do not observe any remarkable changes in the surface properties of the microchannels. MilliQ water and PDMS prepolymeric blends are used as the continuous and dispersed phase, respectively. The Zonyl® fluorosurfactant is dissolved in the aqueous phase (1 wt%) and tested for the formation and stabilization of the droplet emulsions. The two immiscible fluids are injected into the microchannels at constant flow rates, controlled by syringe pumps (model 33, Harvard Apparatus Co.). The PDMS droplets formed are collected in a glass vial through a silicone tube (Tygon® Microbore Tubing) connected to the outlet of the microfluidic device.

### Modelling

The elastomeric microsphere is discretized with linear 8-node brick elements. For the treatment of the contact problem in the discretized setting, the classical node-to-surface approach is adopted with the sphere surface defined as slave.[29] The non-linear problem is consistently linearized with the automatic differentiation technique in the ambient AceGen/AceFem within Mathematica®, and solved using an incremental displacement-control procedure with adaptive time-stepping.

### Measurements, patterning, and analytical methods

To record movies of the droplet formation an inverted microscope (IX-71, Olympus) is coupled with a still (Nikon Digital Camera D40) and a high-speed camera (MONO, Photron FASTCAM APX RS). Scanning electron microscopy (SEM) is carried out using a Raith 150 electron-beam system. The mechanical characterization of PDMS microparticles and films is performed by force–distance spectroscopy using a Nanoscope

 

IIIa system ($Si_3N_4$ tips with an elastic nominal constant of 0.32 N $m^{-1}$). The deformation depth of the tip into the sample surface, $\delta$, is calculated as the difference between the cantilever deflection and the *Z*-displacement (inset of Fig. 2e) of the piezo-scanner, after subtracting the deflection and displacement offsets.[30] Printing experiments are performed using 0.3–3.5 mM water and ethanol solutions of fluorescent dyes and immersing particles for at least 3 hours. Multilevel printing experiments are performed using a combination of fluorescent dye molecules and confocal microscopy (Olympus FV1000) imaging. The samples are excited using an Ar laser source (VFC SP 2009, CVI Melles Griot) emitting at a wavelength of 458 nm for coumarin and 515 nm for rhodamine.

## Acknowledgements

Dr A. Polini is gratefully acknowledged for confocal imaging. C. Maruccio and L. De Lorenzis acknowledge the support from the Italian MIUR through the project FIRB Futuro in Ricerca 2010 "Structural mechanics models for renewable energy applications" (RBFR107AKG).

## References

1 M. Geissler and Y. Xia, *Adv. Mater.*, 2004, **16**, 1249.
2 Y. N. Xia and G. M. Whitesides, *Annu. Rev. Mater. Sci.*, 1998, **28**, 153.
3 A. Perl, D. N. Reinhoudt and J. Huskens, *Adv. Mater.*, 2009, **21**, 2257.
4 A. Bernard, J. P. Renault, B. Michel, H. R. Bosshard and E. Delamarche, *Adv. Mater.*, 2000, **12**, 1067.
5 R. B. A. Sharpe, B. J. F. Titulaer, E. Peeters, D. Burdinski, J. Huskens, H. J. W. Zandvliet, D. N. Reinhoudt and B. Poelsema, *Nano Lett.*, 2006, **6**, 1235.
6 Y. Xia, D. Qin and G. M. Whitesides, *Adv. Mater.*, 1996, **8**, 1015.
7 T. Chen, R. Jordan and S. Zauscher, *Small*, 2011, **7**, 2148.
8 A. Bietsch and B. Michel, *J. Appl. Phys.*, 2000, **88**, 4310.
9 A. Mirkin, *ACS Nano*, 2007, **1**, 79.
10 H. Zhang, R. Elghanian, N. A. Amro, S. Disawal and R. Eby, *Nano Lett.*, 2004, **4**, 1649.
11 D. Dendukuri and P. S. Doyle, *Adv. Mater.*, 2009, **21**, 1, and references within.
12 S. Peng, M. Zhang, X. Niu, W. Wen, P. Sheng, Z. Liu and J. Shi, *Appl. Phys. Lett.*, 2008, **92**, 012108.
13 K. Jiang, P. C. Thomas, S. P. Forry, D. L. DeVoe and S. R. Raghavan, *Soft Matter*, 2012, **8**, 923.
14 R. K. Shah, H. C. Shum., A. C. Rowat, D. Lee, J. J. Agresti, A. S. Utada, L.-Y. Chu, J.-W. Kim, A. Fernandez-Nieves, C. J. Martinez and D. A. Weitz, *Mater. Today*, 2008, **11**, 18.
15 E. Delamarche, H. Schmid, A. Bietsch, N. B. Larsen, H. Rothuizen, B. Michel and H. Biebuyck, *J. Phys. Chem. B*, 1998, **102**, 3324.
16 R. K. Workman and S. Manne, *Langmuir*, 2004, **20**, 805.
17 L. Weeks, A. Noy, A. E. Miller and J. J. De Yoreo, *Phys. Rev. Lett.*, 2002, **88**, 255505.
18 S. Tan, R. L. Sherman Jr and W. T. Ford, *Langmuir*, 2004, **20**, 7015.
19 D. Pisignano, G. Maruccio, E. Mele, L. Persano, F. Di Benedetto and R. Cingolani, *Appl. Phys. Lett.*, 2005, **87**, 123109.
20 W. Xu, N. Chahine and T. Sulchek, *Langmuir*, 2011, **27**, 8470.
21 R. W. Ogden, *Nonlinear Elastic Deformations*, Dover, New York, 1997.
22 H.-W. Li, B. V. O. Muir, G. Fichet and W. T. S. Huck, *Langmuir*, 2003, **19**, 1963.
23 T. M. Squires and S. R. Quake, *Rev. Mod. Phys.*, 2005, **77**, 977.
24 J. A. Helmuth, H. Schmid, R. Stutz, A. Stemmer and H. Wolf, *J. Am. Chem. Soc.*, 2006, **128**, 9296.
25 S. Pagliara, L. Persano, A. Camposeo, R. Cingolani and D. Pisignano, *Nanotechnology*, 2007, **18**, 175302.
26 F. Huo, Z. Zheng, G. Zheng, L. R. Giam, H. Zhang and C. A. Mirkin, *Science*, 2008, **321**, 1658.
27 K.-H. Kim, N. Moldovan and H. D. Espinosa, *Small*, 2005, **1**, 632.
28 J. C. McDonald, D. C. Duffy, J. R. Anderson, D. T. Chiu, H. K. Wu, O. J. A. Schueller and G. M. Whitesides, *Electrophoresis*, 2000, **21**, 27.
29 G. Zavarise and L. De Lorenzis, *Comput. Meth. Appl. Mech. Eng.*, 2009, **198**, 3428.
30 A. Touhami, B. Nysten and Y. F. Dufrêne, *Langmuir*, 2003, **19**, 4539.